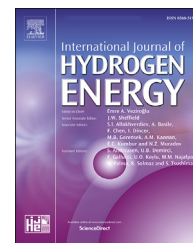




ELSEVIER

Available online at [www.sciencedirect.com](http://www.sciencedirect.com)

ScienceDirect

journal homepage: [www.elsevier.com/locate/hydro](http://www.elsevier.com/locate/hydro)

# (Fe, Ni)S<sub>2</sub>@MoS<sub>2</sub>/NiS<sub>2</sub> hollow heterostructure nanocubes for high-performance alkaline water electrolysis

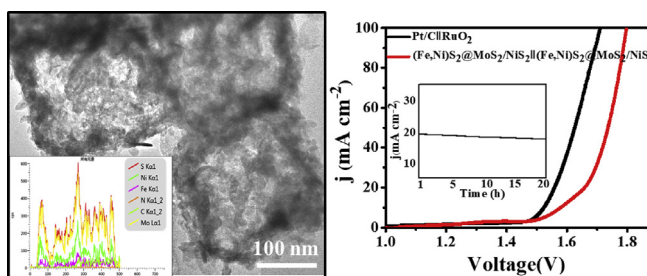
Liangyu Tong, Yunpeng Liu, Chenyu Song, Yuqing Zhang, Sanjay S. Latthe, Shanhu Liu<sup>\*</sup>, Ruimin Xing<sup>\*\*</sup>

Henan Joint International Research Laboratory of Environmental Pollution Control Materials, Henan Key Laboratory of Polyoxometalate Chemistry, College of Chemistry and Chemical Engineering, Henan University, Kaifeng, 475004, PR China

## HIGHLIGHTS

- (Fe, Ni)S<sub>2</sub>@MoS<sub>2</sub>/NiS<sub>2</sub> hollow nanocubes derived from FeNi PBA were obtained.
- The hybrid presents abundant heterointerfaces with maximizing active sites.
- The inner hollow (Fe,Ni)S<sub>2</sub> nanocubes facilitate electrolyte ion diffusion.
- Superior catalytic activity for HER ( $\eta_{50} = 176$  mV) and OER ( $\eta_{50} = 342$  mV) is achieved.
- The stability and durability are greatly enhanced under harsh electrochemical conditions.

## GRAPHICAL ABSTRACT



## ARTICLE INFO

### Article history:

Received 10 August 2021

Received in revised form

5 January 2022

Accepted 21 January 2022

Available online 17 February 2022

### Keywords:

Heterointerface

Bifunctional electrocatalyst

## ABSTRACT

Hollow hybrid heterostructures are regarded to be promising materials as bifunctional electrocatalysts for highly efficient water electrolysis due to their intriguing morphological features and remarkable electrochemical properties. Herein, with FeNi-PBA as both a precursor and morphological template, we demonstrate the rational construct of cost-effective (Fe,Ni)S<sub>2</sub>@MoS<sub>2</sub>/NiS<sub>2</sub> hollow hybrid heterostructures as bifunctional electrocatalysts for alkaline overall water splitting. Microstructural analysis shows that the hybrid is a kind of hierarchical heterostructure composed of MoS<sub>2</sub>/NiS<sub>2</sub> nanosheets/nanoparticles in situ grown on hollow (Fe,Ni)S<sub>2</sub> nanocubes with abundant heterointerfaces, which effectively maximizes the electrochemical active sites to the accessible electrolyte ions, leading to the promoted charge transfer. As expected, the hybrid shows remarkable

<sup>\*</sup> Corresponding author.

<sup>\*\*</sup> Corresponding author.

E-mail addresses: [liushanhu@vip.henu.edu.cn](mailto:liushanhu@vip.henu.edu.cn) (S. Liu), [rmxing@henu.edu.cn](mailto:rmxing@henu.edu.cn) (R. Xing).

<https://doi.org/10.1016/j.ijhydene.2022.01.161>

0360-3199/© 2022 Hydrogen Energy Publications LLC. Published by Elsevier Ltd. All rights reserved.

Overall water splitting  
Alkaline water electrolysis  
NiS<sub>2</sub>  
MoS<sub>2</sub>

alkaline electrocatalytic performance, such as hydrogen evolution overpotential of 176 mV and oxygen evolution overpotential of 342 mV at 50 mA cm<sup>-2</sup>, as well a cell voltage of 1.65 V at 20 mA cm<sup>-2</sup>. Moreover, the stability and durability are greatly enhanced under harsh electrochemical conditions. This study opens a new venue for developing earth-abundant bifunctional electrocatalysts with hollow hybrid heterostructures for alkaline water electrolysis in the future.

© 2022 Hydrogen Energy Publications LLC. Published by Elsevier Ltd. All rights reserved.

## Introduction

Electrochemical water splitting delivers a favorable route to generate clean and sustainable hydrogen fuel from aqueous solution [1–6]. It mainly consists of two half reactions including hydrogen evolution reaction (HER) and oxygen evolution reaction (OER) which needs very competent electrocatalysts for splitting water into H<sub>2</sub> and O<sub>2</sub>. Current noble metal-based electrocatalysts such as Pt-based catalyst for HER and Ir/Ru-based oxides for OER still hold the benchmark. Nevertheless, it remains a big challenge to manufacture such kind noble metal-based electrocatalysts for commercial applications due to the less abundance and high cost [7]. Therefore, the exploration of noble metal-free materials as electrocatalysts for HER and OER has been extensively pursued, such as transition-metal sulfides [8–12], oxides/hydroxides [13], carbides [14], nitrides [15], and phosphides [16–19].

Among transition metal sulfides, molybdenum disulfide becomes a star material for acid HER catalysis, due to its unsaturated edge active sites like Pt favoring hydrogen absorption and unique layered graphene-like structure facilitating electron transfer [20–22]. However, MoS<sub>2</sub> exhibits unsatisfactory alkaline HER catalytic activity and also is inert for alkaline OER, which limited its application as bifunctional electrocatalysts [2]. On the other hand, nickel sulfide is regarded as OER-active electrocatalyst owing to the facilitated chemisorption towards oxygen-containing species; but its HER catalytic activity is not up to the mark. Therefore, hybridizing NiS<sub>2</sub> with MoS<sub>2</sub> is supposed to be a promising approach to fabricate heterostructure bifunctional catalysts with high HER and OER activities in the alkaline electrolyte [9,23,24].

Hollow hybrid heterostructures possess unique features such as large specific surface area with abundant exposure of active sites, shortened length of electrolyte ion diffusion with facilitated charge transfer at the interface, which are beneficial for achieving superior electrocatalytic activity for HER/OER [25]. Recently, Prussian blue analogues (PBAs) receive great interest as the precursors in terms of the preparation of hollow and core-shell hybrid structure due to their facile synthesis and unique porous feature [26]. Furthermore, the electronic structure of PBA-derived materials could be regulated by varying the metallic composition and doping heteroatoms, which produces tailorable properties like abundant exposed facets to the accessible catalytic sites, high surface area to facilitate electron transport, thus improving electrochemical activity [27,28].

Taking all these points into account, herein, with FeNi-PBA as both a precursor and morphological template, we designed cost-effective (Fe,Ni)S<sub>2</sub>@MoS<sub>2</sub>/NiS<sub>2</sub> hollow hybrid heterostructure as bifunctional electrocatalyst for alkaline overall water splitting. Microstructural analysis shows that the hybrid is a kind of hierarchical heterostructure composed of MoS<sub>2</sub>/NiS<sub>2</sub> nanosheets/nanoparticles *in situ* grown on hollow (Fe,Ni)S<sub>2</sub> nanocubes, which effectively maximize the electrochemical active sites to the accessible electrolyte ions, leading to the promoted charge transfer. As expected, the hybrid shows remarkable alkaline HER and OER electrocatalytic performance. Moreover, the stability and durability are investigated under harsh electrochemical conditions.

## Experimental method

### Materials

Nickel sulfate hexahydrate (NiSO<sub>4</sub>·6H<sub>2</sub>O), sodium citrate dehydrate (Na<sub>3</sub>C<sub>6</sub>H<sub>5</sub>O<sub>7</sub>·2H<sub>2</sub>O), potassium ferricyanide (K<sub>3</sub>[Fe(CN)<sub>6</sub>]), ethanol, thioacetamide (C<sub>2</sub>H<sub>5</sub>NS, named as TAA), nickel (II) nitrate hexahydrate [Ni(NO<sub>3</sub>)<sub>2</sub>·6H<sub>2</sub>O], sodium molybdate (VI) dihydrate [Na<sub>2</sub>MoO<sub>4</sub>·2H<sub>2</sub>O], sulfur powder were purchased from Aladdin Chemical Co. Ltd. All the reagents are analytical grade and used without further purification.

### Synthesis of solid and hollow FeNi prussian blue analogue (FeNi-PBA)

Typically, 1 mmol of NiSO<sub>4</sub>·6H<sub>2</sub>O and 1.25 mmol of Na<sub>3</sub>C<sub>6</sub>H<sub>5</sub>O<sub>7</sub>·2H<sub>2</sub>O were dissolved in 50 mL of deionized water to form solution A. Then, 0.7 mmol of K<sub>3</sub>[Fe(CN)<sub>6</sub>] was dissolved in 10 mL of deionized water to form solution B. Solutions A and B were thoroughly mixed under magnetic stirring for precipitation and aged for 20 h. The precipitate was washed three times and dried at 50 °C for 12 h to obtain solid FeNi-PBA nanocubes. Thirty milligrams of solid FeNi-PBA nanocubes were dispersed in 10 mL of ethanol under ultrasonication for 30 min to obtain a uniform solution. Then, 5 mL of thioacetamide solution (5 mg/mL) was dropped into the above suspension under magnetic stirring. Afterwards, the mixture was transferred to 25 mL of autoclave and kept at 150 °C for 12 h. Then the precipitate was thoroughly washed and then dried at 60 °C for overnight to obtain hollow FeNi-PBA nanocubes.

## Synthesis of hollow FeNi-PBA@NiMoO<sub>4</sub> and (Fe,Ni)<sub>S<sub>2</sub></sub>@MoS<sub>2</sub>/NiS<sub>2</sub>

Twenty milligrams of the above hollow FeNi PBA were dispersed in 16 mL of deionized water under ultrasonication for half an hour to obtain a uniform solution. Then, 100 mg of Ni(NO<sub>3</sub>)<sub>2</sub>·6H<sub>2</sub>O, 80 mg of Na<sub>2</sub>MoO<sub>4</sub>·2H<sub>2</sub>O were added the suspension slowly. Afterwards, the mixed solution was transferred to a 25 mL Teflon-lined stainless steel autoclave and heated to 120 °C for 6 h. The obtained hollow FeNi-PBA@NiMoO<sub>4</sub> precursors were washed by distilled water and ethanol several times, and dried at 60 °C overnight. Finally, sublimed sulfur and FeNi-PBA@NiMoO<sub>4</sub> precursors were put at the upstream and downstream side of the tube furnace, then the furnace was heated to 350 °C for 2 h with a ramp rate of 5 °C under N<sub>2</sub> atmosphere to obtain the hollow (Fe,Ni)<sub>S<sub>2</sub></sub>@MoS<sub>2</sub>/NiS<sub>2</sub> heterostructures.

### Materials characterization

Powder X-ray diffraction (XRD) data are collected on an X-ray D8 Advance instrument (Bruker, Germany). Scanning electron microscopy (SEM) is carried on a JSM-7610 F scanning electron microscope (Hitachi). Transmission electron microscopy (TEM) is performed on a JEOL JEM-2100 transmission electron microscope, equipped with energy dispersive X-ray (EDX) analyzer. Gatan Microscopy Suite Software is used for HRTEM analysis. X-ray photoelectron spectroscopy (XPS) analysis is performed on a Thermo Scientific Escalab 250Xi equipped with 150 W monochromatized Al K<sub>α</sub> radiation (hν = 1486.6 eV), where all peaks are referred to the signature C1s peak for adventitious carbon at 284.8 eV. Quantachrome Nova-1000 surface analyzer is used to analyze the surface area and the pore size of the prepared catalysts.

### Electrochemical characterization

The HER and OER electrochemical behaviors of the synthesized samples are analyzed in a three-electrode setup at CHI 760 E electrochemical work station and two-electrode system is used to investigate the overall water splitting. The working composite electrode is fabricated by adding 2 mg of the synthesized material into a mixture of Nafion (30 μL) and ethanol (370 μL) and being sonicated for 30 min to make a homogenous ink. The acquired ink is drop-casted on (1 × 1 cm<sup>2</sup>) nickel foam substrate and then dried at 60 °C overnight. Linear sweep voltammetry (LSV) with a scan rate of 2 mV/s is conducted in 1 M KOH as the electrolyte solution using a platinum wire and Hg/HgO as the counter and the reference electrodes, respectively. Afterwards, all the potential values are converted to values with reference to a reversible hydrogen electrode (RHE). To determine the double-layer capacitance (C<sub>dl</sub>), cyclic voltammetry (CV) taken with various scan speeds are carried out in the potential window of 1.0–1.1 V vs. RHE. Electrochemical impedance spectroscopy (EIS) is achieved in the same setup at open circuit voltage in the frequency range of 100 Hz to 100 kHz with an AC voltage of 5 mV.

## Results and discussion

Hollow (Fe, Ni)<sub>S<sub>2</sub></sub>@MoS<sub>2</sub>/NiS<sub>2</sub> heterostructures are prepared via step-by-step procedures. SEM observation and XRD patterns are used to confirm the morphologies and crystal phase of the respective products. Firstly, solid FeNi-PBA is synthesized via a conventional precipitation method at room temperature. SEM observation shows solid FeNi-PBA are mono-dispersed and uniform nanocubes with smooth surface (Fig. 1a). Then, hollow FeNi-PBA nanocubes are obtained with solid FeNi-PBA as precursor after selective etching of TAA under hydrothermal conditions; hollow FeNi-PBA still exhibits nanocube feature but with rough surface and visible pores (Fig. 1b). Afterwards, hollow FeNi-PBA@NiMoO<sub>4</sub> is prepared when hollow FeNi-PBA nanocubes with rough surfaces act as substrate via further hydrothermal treatment in the presence of nickel and molybdenum sources; SEM observation shows NiMoO<sub>4</sub> nanosheets vertically grow on hollow FeNi-PBA nanocubes (Fig. 1c). At last, hollow (Fe, Ni)<sub>S<sub>2</sub></sub>@MoS<sub>2</sub>/NiS<sub>2</sub> is obtained via vapor deposition in the tube furnace when sublimed sulfur and FeNi-PBA@NiMoO<sub>4</sub> are put at the upstream and downstream side; As expected, MoS<sub>2</sub> nanosheets together with NiS<sub>2</sub> nanoparticles growing on hollow (Fe, Ni)<sub>S<sub>2</sub></sub> nanocubes to form such a hybrid is achieved (Fig. 1d). In contrast, rod-like MoS<sub>2</sub>/NiS<sub>2</sub> nanostructures are obtained by direct sulphurization of NiMoO<sub>4</sub> precursors in the tube furnace (Fig. S1a); Whereas (Fe, Ni)<sub>S<sub>2</sub></sub> is prepared by sulphurization of hollow FeNi-PBA nanocubes in the tube furnace (Fig. S1b).

Their respective XRD patterns are displayed in Fig. S2 It is noticeable that the XRD patterns of (Fe,Ni)<sub>S<sub>2</sub></sub> nanocubes match well with the standard iron nickel sulfide (JCPDS card No. 02–0850) [29]. The diffraction peaks of MoS<sub>2</sub>/NiS<sub>2</sub> match well with MoS<sub>2</sub> (JCPDS card No: 37–1492) [30] and NiS<sub>2</sub> (JCPDS card No: 11–0099) [31]. Whereas the XRD patterns of (Fe, Ni)<sub>S<sub>2</sub></sub>@MoS<sub>2</sub>/NiS<sub>2</sub> show well-resolved intense peaks of three different crystal phases including (Fe, Ni)<sub>S<sub>2</sub></sub>, MoS<sub>2</sub> and NiS<sub>2</sub>. It is worth noting that the intensity of MoS<sub>2</sub> (002) diffraction peak in (Fe, Ni)<sub>S<sub>2</sub></sub>@MoS<sub>2</sub>/NiS<sub>2</sub> seems decreased compared to pristine MoS<sub>2</sub>/NiS<sub>2</sub>, presumably suggesting the rough surfaces of (Fe,Ni)<sub>S<sub>2</sub></sub> nanocubes effectively inhibit the exfoliated growth of MoS<sub>2</sub> into fewer layers. The fewer layers of MoS<sub>2</sub> would expose more catalytically active edged sites to accelerate the electron transport, which is favorable to HER reaction [2].

TEM images of (Fe,Ni)<sub>S<sub>2</sub></sub>@MoS<sub>2</sub>/NiS<sub>2</sub> display the morphology feature of hollow nanocubes with the size of about 230 nm (Fig. 2a). X-ray energy dispersive spectra (EDS) analysis (Fig. 2b) shows that the atomic ratio of total metals (Fe, Ni and Mo) to sulfur is 2.26, slightly higher than the stoichiometric composition of (Fe,Ni)<sub>S<sub>2</sub></sub>@MoS<sub>2</sub>/NiS<sub>2</sub>, an indicative evidence of the presence of abundant sulfur. HRTEM image gives the detailed information of the mixed crystal phases (Fig. 2c). The lattice fringes of 0.25 nm and 0.63 nm belong to the (200) crystal plane of NiS<sub>2</sub> and (002) crystal plane of MoS<sub>2</sub>, respectively. While the lattice fringes with spacing of 0.19 and 0.28 nm correspond to the (220) and (200) crystal planes of (Fe, Ni)<sub>S<sub>2</sub></sub>, respectively. Besides, EDX mapping analyses (Fig. 2d) corroborate the distribution of S,

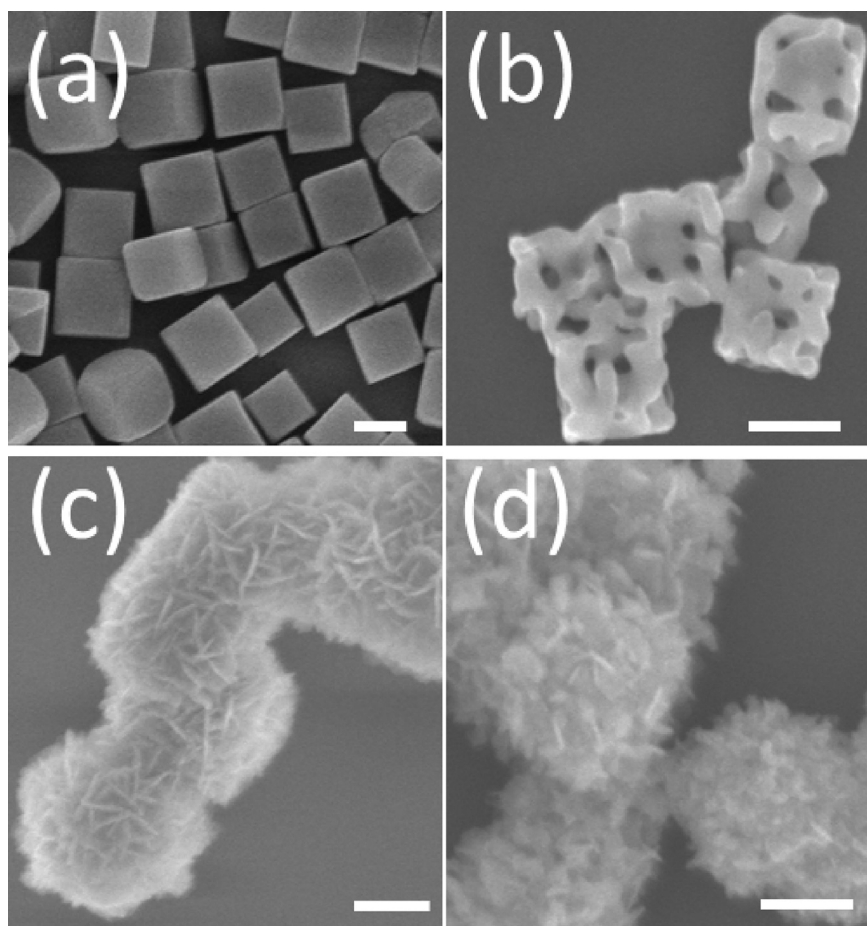


**Fig. 1** – SEM images of solid FeNi-PBA nanocubes (a), hollow FeNi-PBA nanocubes (b), hollow FeNi-PBA@NiMoO<sub>4</sub> (c), and hollow (Fe, Ni)S<sub>2</sub>@MoS<sub>2</sub>/NiS<sub>2</sub> (d). The scale bar is 200 nm.

Mo, Ni and Fe elements in the hybrid with obvious rich sulfur. These above evidences confirm that MoS<sub>2</sub>/NiS<sub>2</sub> nanosheets/nanoparticles grow on the hollow (Fe,Ni)S<sub>2</sub> nanocubes, in which MoS<sub>2</sub>/NiS<sub>2</sub> nanosheets/nanoparticles provide the abundant active sites, while hollow (Fe,Ni)S<sub>2</sub> nanocubes accelerate the electrolyte diffusion, as well as the strong interfacial coupling due to the abundant heterointerfaces between MoS<sub>2</sub>, NiS<sub>2</sub> and (Fe,Ni)S<sub>2</sub>, thus synergistically boosting the electrochemical water splitting performance.

X-ray photoelectron spectroscopy (XPS) measurements are used to analyze the elemental species and their respective electronic states of (Fe,Ni)S<sub>2</sub>@MoS<sub>2</sub>/NiS<sub>2</sub>, with those of pristine (Fe,Ni)S<sub>2</sub> and MoS<sub>2</sub>/NiS<sub>2</sub> for comparison. The XPS survey spectra of (Fe,Ni)S<sub>2</sub>@MoS<sub>2</sub>/NiS<sub>2</sub> confirm all the presence of Ni, Fe, S and Mo elements (Fig. S3). As shown in Fig. 3a, Ni 2p core level spectra exhibit two spin-orbit doublets and two shakeup satellite (Sat.) peaks. The Ni<sup>2+</sup> (853.5 eV for 2p<sub>3/2</sub> and 871.0 eV for 2p<sub>1/2</sub>) and Ni<sup>3+</sup> (856.3 eV for 2p<sub>3/2</sub> and 875.5 eV for 2p<sub>1/2</sub>) photoelectron peaks in MoS<sub>2</sub>/NiS<sub>2</sub> and (Fe,Ni)S<sub>2</sub> give certain positive shifts to those peaks in the hybrid (Fe,Ni)S<sub>2</sub>@MoS<sub>2</sub>/NiS<sub>2</sub> [29]. For deconvoluted Mo 3d profiles (Fig. 3b), the fitting analysis shows that two main peaks located at 228.85 and 232.25 eV are attributed to the 3d<sub>5/2</sub> and 3d<sub>3/2</sub> of Mo<sup>4+</sup> ions, while the band at 235.7 eV corresponds to Mo<sup>6+</sup> due to the partial air oxidation. Moreover, another weak peak centered at 226.15 eV corresponds to S 2s states [2]. Compared to pristine

MoS<sub>2</sub>/NiS<sub>2</sub>, these three peaks including Mo 3d<sub>5/2</sub>, Mo 3d<sub>3/2</sub> and Mo–S in the hybrid (Fe,Ni)S<sub>2</sub>@MoS<sub>2</sub>/NiS<sub>2</sub> are slightly upshifted (229.05, 232.6 and 226.7 eV) [23]. In Fe 2p high resolution spectra (Fig. 3c), the Fe 2p<sub>3/2</sub> (709.2 eV for Fe<sup>2+</sup> and 712.8 eV for Fe<sup>3+</sup>) and 2p<sub>1/2</sub> (723.1 eV for Fe<sup>2+</sup> and 727.2 eV for Fe<sup>3+</sup>) photoelectron peaks in pristine (Fe,Ni)S<sub>2</sub> also give certain positive shifts to those peaks in the hybrid (Fe,Ni)S<sub>2</sub>@MoS<sub>2</sub>/NiS<sub>2</sub> [32]. These different degrees of shifts of their respective photoelectron peaks in (Fe,Ni)S<sub>2</sub>@MoS<sub>2</sub>/NiS<sub>2</sub> indicate the occurrence of electron interaction between MoS<sub>2</sub>/NiS<sub>2</sub> and (Fe,Ni)S<sub>2</sub>, presumably resulting from the formation of intimate heterointerfaces within the hybrid. In addition, peak deconvolution of S 2p (Fig. 3d) indicates that one doublet at 161.8 eV and 163.2 eV correspond to 2p<sub>3/2</sub> and 2p<sub>1/2</sub> of sulfide species (S<sup>2-</sup>). The other doublet emerged at 162.6 eV and 163.9 eV is related to 2p<sub>3/2</sub> and 2p<sub>1/2</sub> of sulfur bridge species (bridging S<sub>2</sub><sup>2-</sup>) in terminal edges with undercoordinated Mo–S sites. The peak at 169.25 eV is assigned to S–O species resulting from the surface air exposure. The terminal disulfide sites are regarded to be involved in reducing protons during the HER, which was beneficial for electrocatalytic reaction [2].

Furthermore, the surface area of (Fe,Ni)S<sub>2</sub>@MoS<sub>2</sub>/NiS<sub>2</sub> is investigated by N<sub>2</sub> adsorption-desorption isotherms with (Fe, Ni)S<sub>2</sub> and MoS<sub>2</sub>/NiS<sub>2</sub> for comparison. As displayed in, Fig. S4 (Fe, Ni)S<sub>2</sub>@MoS<sub>2</sub>/NiS<sub>2</sub> as well as (Fe, Ni)S<sub>2</sub> and MoS<sub>2</sub>/NiS<sub>2</sub> exhibit a type IV isotherm curve, an indicative of the

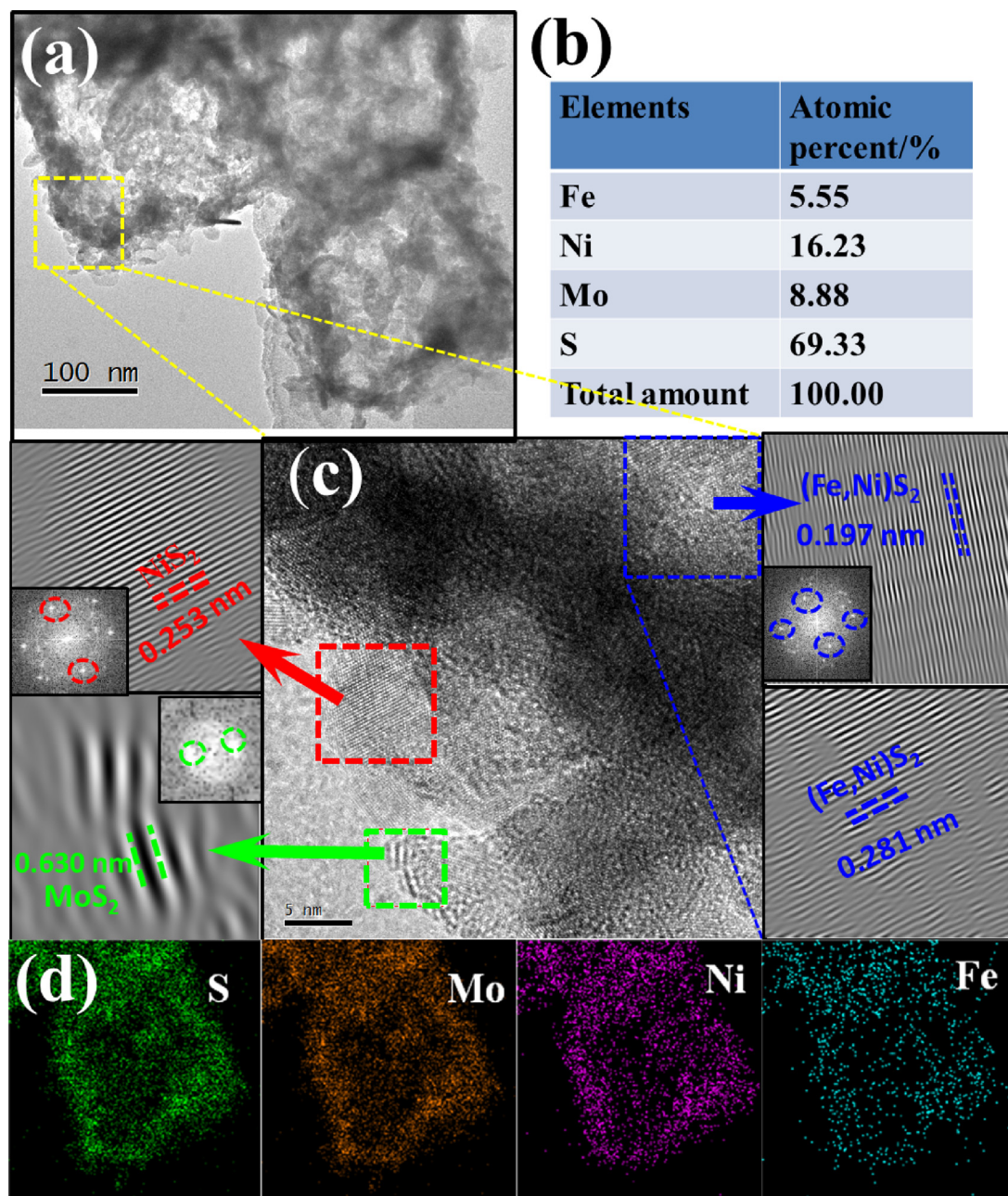


Fig. 2 – TEM image (a), EDX analysis (b), high resolution TEM image (c) and their corresponding elemental mapping (d) of hollow (Fe, Ni) $S_2$ @MoS $_2$ /NiS $_2$  heterostructures.

mesoporous structure. Brunauer-Emmett-Teller (BET) surface area of (Fe,Ni) $S_2$ @MoS $_2$ /NiS $_2$  is found to be 65.1 m $^2$ /g, far larger than those of (Fe, Ni) $S_2$  (40.5 m $^2$ /g) and MoS $_2$ /NiS $_2$  (32.9 m $^2$ /g). Therefore, the higher surface area and mesoporous nature of (Fe,Ni) $S_2$ @MoS $_2$ /NiS $_2$  ensure the exposure of enriched active sites, which is beneficial to enhance charge transfer rates and superior contact towards the electrolyte solution, thus improving the electrochemical behaviors.

#### Hydrogen evolution activity

The HER catalytic activities of (Fe, Ni) $S_2$ @MoS $_2$ /NiS $_2$  is investigated by the polarization curves from linear sweep

voltammetry (LSV) in 1.0 M KOH electrolyte using a three electrode system at a scan rate of 2 mV/s. For comparison, we also evaluated the electrocatalytic performance of commercial Pt/C (20 wt%), Ni Foam, (Fe, Ni) $S_2$  and MoS $_2$ /NiS $_2$ . As displayed in Fig. 4a, Pt/C on NF undoubtedly exhibits the best performance with a low overpotential of 35 mV at 10 mA cm $^{-2}$  whereas bare Ni foam shows negligible catalytic activity. (Fe, Ni) $S_2$ @MoS $_2$ /NiS $_2$  shows superior catalytic performance toward HER, with a cathodic current density of 10 and 50 mA cm $^{-2}$  at a low overpotential of 91 and 176 mV. The catalytic performance of (Fe,Ni) $S_2$ @MoS $_2$ /NiS $_2$  is obviously higher than that of (Fe, Ni) $S_2$  ( $\eta_{10}$  = 199 mV) and MoS $_2$ /NiS $_2$  ( $\eta_{10}$  = 163 mV). Moreover, (Fe, Ni) $S_2$ @MoS $_2$ /NiS $_2$  exhibits the

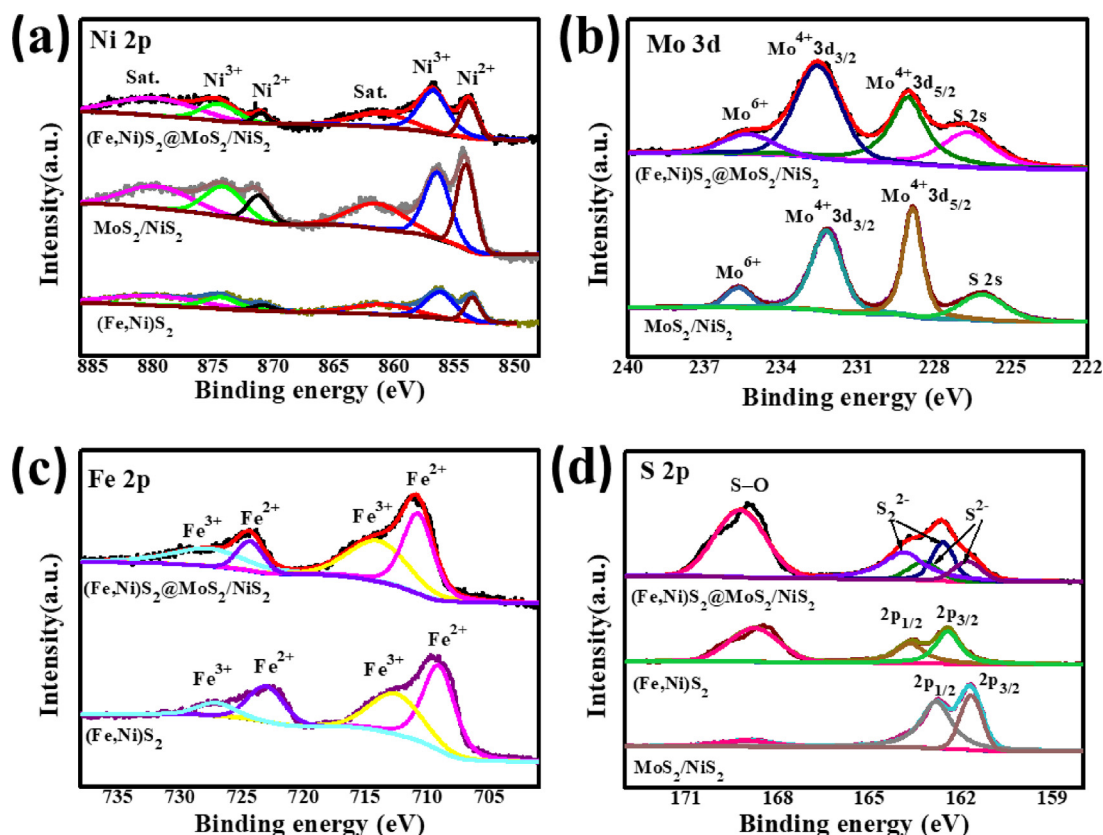


**Fig. 3** – High resolution XPS spectra: Ni 2p (a), Mo 3d (b), Fe 2p (c) and S 2p (d) of hollow  $(\text{Fe, Ni})\text{S}_2@\text{MoS}_2/\text{NiS}_2$ , with  $(\text{Fe, Ni})\text{S}_2$  and  $\text{MoS}_2/\text{NiS}_2$  for comparison.

competitive electrocatalytic activities, compared to the previous reported  $\text{MoS}_2$ -based catalysts in alkaline media at  $10 \text{ mA cm}^{-2}$ , such as  $(\text{Ni, Fe})\text{S}_2@\text{MoS}_2$  ( $130 \text{ mV}$ ) [29],  $\text{MoS}_2/\text{Co}_9\text{S}_8/\text{Ni}_3\text{S}_2/\text{Ni}$  foam<sup>36</sup> ( $113 \text{ mV}$ ) [33],  $\text{MoS}_2/\text{Ni}_3\text{S}_2$  heterostructures ( $110 \text{ mV}$ ) [8],  $\text{NiS}-\text{MoS}_2$  hetero-nanosheet arrays ( $106 \text{ mV}$ ) [34] and roughly the same as  $\text{MoS}_2-\text{Ni}_3\text{S}_2$  hetero-nanorods ( $98 \text{ mV}$ ) [35]. The low overpotential of  $(\text{Fe, Ni})\text{S}_2@\text{MoS}_2/\text{NiS}_2$  is mainly due to the presence of abundant heterointerfaces with catalytically active sites for superior electrocatalytic reaction. Therefore, the hybrid is a promising candidate for HER electrocatalyst.

The Tafel slopes derived from the LSV polarization curves is used to investigate the HER reaction kinetics. As shown in Fig. 4b, the Tafel slope of  $(\text{Fe, Ni})\text{S}_2@\text{MoS}_2/\text{NiS}_2$  is approximately  $96.7 \text{ mV dec}^{-1}$ , smaller than that of pristine  $(\text{Fe, Ni})\text{S}_2$  ( $160.7 \text{ mV dec}^{-1}$ ) and  $\text{MoS}_2/\text{NiS}_2$  ( $125.3 \text{ mV dec}^{-1}$ ). The Tafel slope of  $96.7 \text{ mV dec}^{-1}$  for  $(\text{Fe, Ni})\text{S}_2@\text{MoS}_2/\text{NiS}_2$  suggests the HER following the Volmer-Heyrovsky mechanism [8]. Moreover, the catalytic active sites are estimated by the electrochemical surface area (ECSA), which is obtained by CV measurement with different scan rates in a potential range from 0.17 to 0.27 V (vs RHE). The electrochemical double layer capacitance ( $C_{dl}$ ) proportional to the ECSA, as shown in Fig. 4c, is obtained by the slopes of the fitted line at different scan rates. The calculated  $C_{dl}$  values of  $(\text{Fe, Ni})\text{S}_2@\text{MoS}_2/\text{NiS}_2$  is  $33.23 \text{ mF cm}^{-2}$ , superior to those of  $\text{MoS}_2/\text{NiS}_2$  ( $8.47 \text{ mF cm}^{-2}$ ) and  $(\text{Fe, Ni})\text{S}_2$  catalysts ( $1.53 \text{ mF cm}^{-2}$ ). This result indicates that the  $(\text{Fe, Ni})$

$\text{S}_2@\text{MoS}_2/\text{NiS}_2$  catalyst enriches the electrochemical active sites on the electrode surface to the accessible electrolyte ions, due to the unique morphology feature of hollow nanocubes and the maximum exposure of the catalytically active edges of  $\text{MoS}_2$  [9]. Electrochemical impedance spectroscopy (EIS) is performed to investigate the charge-transfer kinetics at the electrode/electrolyte interface. The charge transfer resistance ( $R_{ct}$ ) is determined according to the semicircle nature of recorded EIS curves. As shown in Fig. 4d, the  $(\text{Fe, Ni})\text{S}_2@\text{MoS}_2/\text{NiS}_2$ -modified electrode delivers a lower  $R_{ct}$  value than  $\text{MoS}_2/\text{NiS}_2$ - and  $(\text{Fe, Ni})\text{S}_2$ -modified electrode, which indicates the higher electrical conductivity and faster electron transfer rates on  $(\text{Fe, Ni})\text{S}_2@\text{MoS}_2/\text{NiS}_2$ -modified electrode.

Furthermore, the stability of  $(\text{Fe, Ni})\text{S}_2@\text{MoS}_2/\text{NiS}_2$  is evaluated by LSV and long-time chronoamperometry (*i-t*) measurements (Fig. 4e and f). As shown, the slight deviation of polarization curve is observed after 5000 CV cycles; meanwhile, the current density shows negligible loss after 40 h. These above results show the superior stability and durability of  $(\text{Fe, Ni})\text{S}_2@\text{MoS}_2/\text{NiS}_2$  for HER. The improvement of the HER performance could be ascribed to the following synergetic effects. The inner hollow  $(\text{Fe, Ni})\text{S}_2$  nanocubes is regarded to accelerate the electrolyte diffusion for HER; meanwhile, the outer  $\text{MoS}_2$  nanosheets expose more catalytically active edges, facilitating the electrode/electrolyte contact and thus achieving the high catalytic activity. Therefore,  $(\text{Fe, Ni})\text{S}_2@\text{MoS}_2/\text{NiS}_2$  could be promising as high efficient and stable HER catalyst.

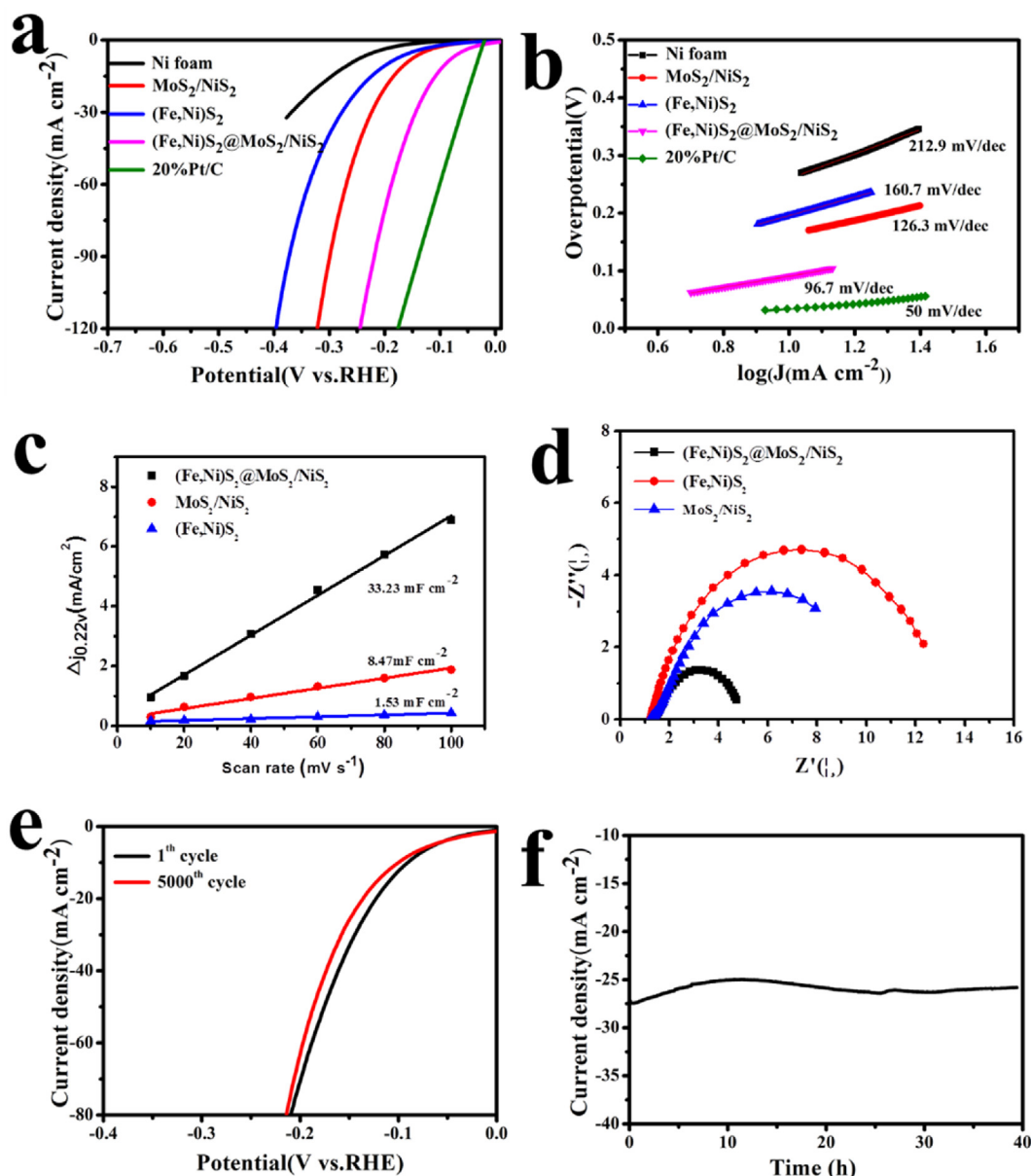


**Fig. 4** – HER polarization curves (a), their corresponding Tafel plots (b), double-layer capacitance (c) and EIS (d) of different samples in 1 M KOH; (e) Polarization curves at the first cycle and after 5000 cycles (e) and stability test for 40 h (f) of (Fe, Ni) S<sub>2</sub>@MoS<sub>2</sub>/NiS<sub>2</sub>.

#### Oxygen evolution activity

The OER performance of (Fe, Ni)S<sub>2</sub>@MoS<sub>2</sub>/NiS<sub>2</sub> catalyst as anode materials was further examined in 1.0 M KOH with a scan rate of 2 mV/s, together with that of RuO<sub>2</sub>, Ni Foam, (Fe, Ni)S<sub>2</sub> and MoS<sub>2</sub>/NiS<sub>2</sub> for comparison. Fig. 5a displays the polarization curves of different modified electrodes. As shown, the (Fe, Ni)S<sub>2</sub>@MoS<sub>2</sub>/NiS<sub>2</sub>-modified electrode exhibit superior OER activity with an impressive overpotential of 342 mV to attain a current density of 50 mA cm<sup>-2</sup>, compared to the state-of-the-art RuO<sub>2</sub> (355 mV at 20 mA cm<sup>-2</sup>), pristine (Fe, Ni)S<sub>2</sub> (330 mV at 20 mA/cm<sup>-2</sup>), MoS<sub>2</sub>/NiS<sub>2</sub> (361 mV at 20 mA/cm<sup>-2</sup>) and Ni foam (419 mV at 20 mA/cm<sup>-2</sup>) catalyst. Fig. 5b gives the calculated Tafel slopes of (Fe, Ni)S<sub>2</sub>@MoS<sub>2</sub>/NiS<sub>2</sub> (58 mV dec<sup>-1</sup>), RuO<sub>2</sub> (81 mV dec<sup>-1</sup>), Ni foam (115 mV

dec<sup>-1</sup>), (Fe, Ni)S<sub>2</sub> (83 mV dec<sup>-1</sup>) and MoS<sub>2</sub>/NiS<sub>2</sub> (89 mV dec<sup>-1</sup>), indicating the (Fe, Ni)S<sub>2</sub>@MoS<sub>2</sub>/NiS<sub>2</sub> has excellent OER activity and better charge transfer coefficient. The stability is proven by the LSV comparison in the initial and after 5000 cyclic potential sweeps with a scan rate of 20 mVs<sup>-1</sup> and long-time chronoamperometry (i-t) measurements of (Fe, Ni)S<sub>2</sub>@MoS<sub>2</sub>/NiS<sub>2</sub> catalyst. When compared to the initial curve, a negligible shift is observed in the overpotential after 5000 cycles (Fig. 5c). Furthermore, the chronoamperometry measurement shows no obvious degradation of current density for 40 h (Fig. 5d), supportive evidence for excellent durability for long-term operation. These results confirm that the excellent electrochemical stability and durability of the (Fe, Ni) S<sub>2</sub>@MoS<sub>2</sub>/NiS<sub>2</sub> catalyst during the OER process in the alkaline electrolyte.

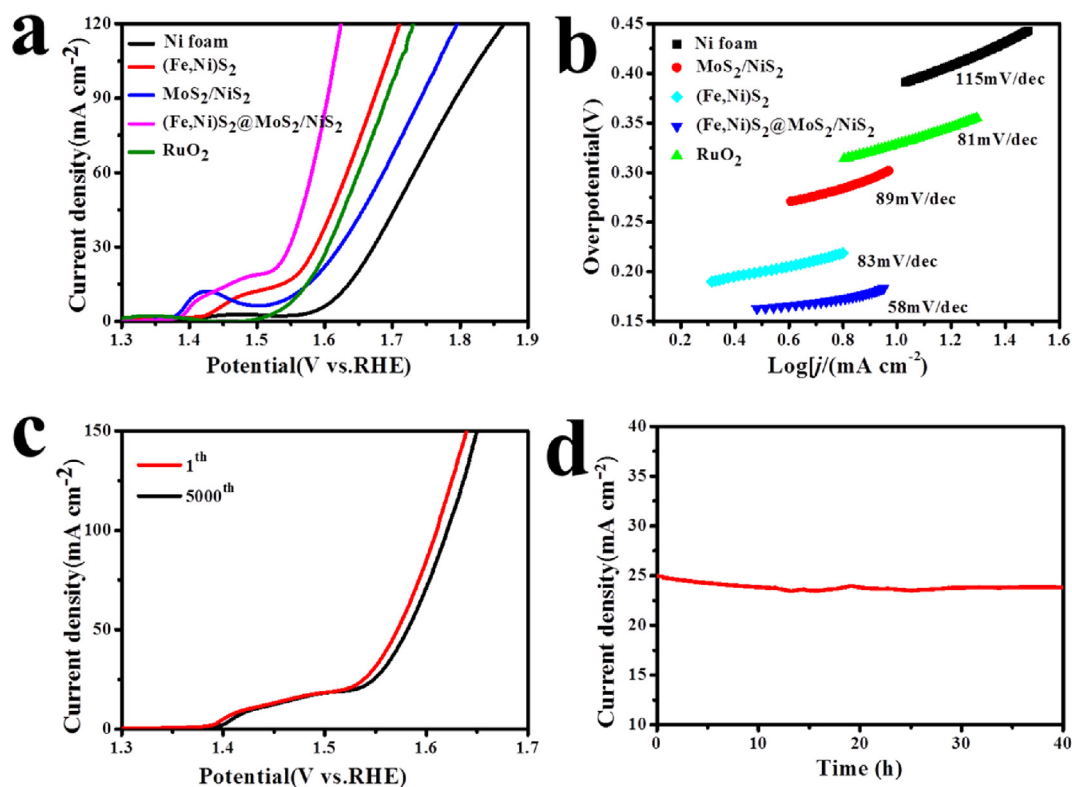


Fig. 5 – OER polarization curves (a) and their corresponding Tafel plots (b) of different modified electrodes in 1 M KOH. Polarization curves before and after 5000 cycles (c) and OER stability test (d) of  $(\text{Fe,Ni})\text{S}_2/\text{MoS}_2/\text{NiS}_2$ .

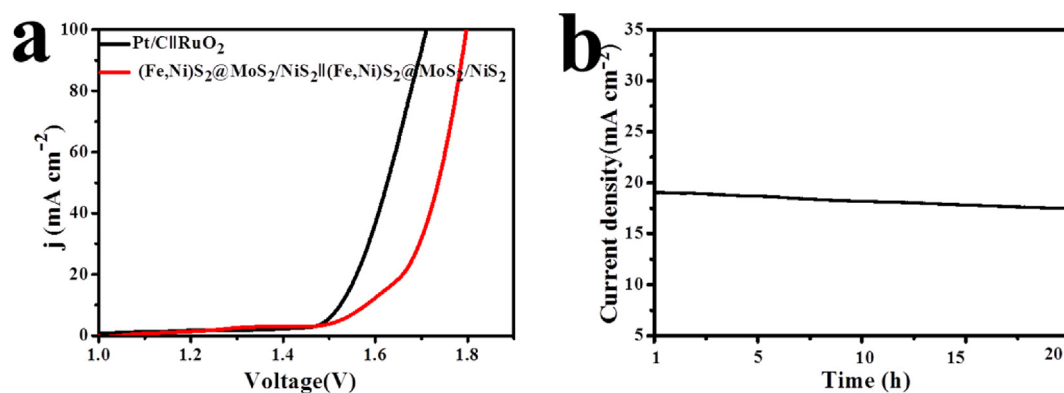


Fig. 6 – Polarization curves of different two-electrode cells (a) and chronoamperometry curves of  $(\text{Fe,Ni})\text{S}_2/\text{MoS}_2/\text{NiS}_2//(\text{Fe,Ni})\text{S}_2/\text{MoS}_2/\text{NiS}_2$  at  $15 \text{ mA cm}^{-2}$  in 1.0 M KOH for 20 h (b).

### Overall water splitting

The above results show the  $(\text{Fe, Ni})\text{S}_2/\text{MoS}_2/\text{NiS}_2$  is active and stable catalyst for HER and OER in alkaline electrolyte. Therefore,  $(\text{Fe, Ni})\text{S}_2/\text{MoS}_2/\text{NiS}_2$  is evaluated simultaneously as bifunctional catalysts for anode and cathode of overall water splitting. The two-electrode cell with  $(\text{Fe, Ni})\text{S}_2/\text{MoS}_2/\text{NiS}_2//(\text{Fe, Ni})\text{S}_2/\text{MoS}_2/\text{NiS}_2$  electrolyzer affords a current density of 10 and  $20 \text{ mA cm}^{-2}$  at cell voltage of 1.57 and 1.65 V, respectively (Fig. 6a), which is comparable to the commercial Pt/C||RuO<sub>2</sub> electrocatalysts and superior to recently reported catalysts. After 20 h of electrolysis, the  $(\text{Fe,Ni})\text{S}_2/\text{MoS}_2/\text{NiS}_2//$

$(\text{Fe,Ni})\text{S}_2/\text{MoS}_2/\text{NiS}_2$  electrolyzer still shows no obvious decay for overall water splitting (Fig. 6b), indicating the high stability over long-term operation. Considering the wide sources and easy preparation of non-noble metal-based electrocatalyst, the hybrid exhibits great potential for large-scale water electrolysis with low cost and high efficiency.

### Conclusions

In summary, this work reports  $(\text{Fe, Ni})\text{S}_2/\text{MoS}_2/\text{NiS}_2$  hollow hybrid heterostructures as active and stable bifunctional

electrocatalyst for overall water splitting to generate both O<sub>2</sub> and H<sub>2</sub> in alkaline solution, which is achieved by the facile and conventional strategies. Benefitted from the maximized exposure of catalytic active edges of MoS<sub>2</sub> nanosheets and NiS<sub>2</sub> nanoparticles (the outer shell) and the inner unique hollow structure of (Fe,Ni)S<sub>2</sub> nanocubes accelerating the electrolyte diffusion, the hybrid exhibits remarkable alkaline electrocatalytic activity with HER overpotential of 176 mV and OER overpotential of 342 mV at 50 mA cm<sup>-2</sup>. A low cell voltage of 1.65 V at 20 mA cm<sup>-2</sup> is required for water electrolysis with satisfactory durability after continuous operation for 20 h. Our work demonstrates that exposing abundant active sites, designing hollow hybrid heterostructures towards earth-abundant electrocatalysts are effective strategies for boosting the electrocatalytic activity.

### Declaration of competing interest

The authors declare that they have no known competing financial interests or personal relationships that could have appeared to influence the work reported in this paper.

### Acknowledgements

The authors gratefully appreciate the support from Science Technology Research Project of Henan province (202102310541, 212102210587 and 212102311039). Also, we express thanks to Dr. Daibing Luo from Analytical & Testing Center of Sichuan University for the valuable discussion and characterization.

### Appendix A. Supplementary data

Supplementary data to this article can be found online at <https://doi.org/10.1016/j.ijhydene.2022.01.161>.

### REFERENCES

- [1] Zhou Y, Fan HJ. Progress and challenge of amorphous catalysts for electrochemical water splitting. *ACS Mater Lett* 2021;3:136–47.
- [2] Liu S, Li S, Sekar K, Li R, Zhu Y, Xing R, et al. Hierarchical ZnS@C@MoS<sub>2</sub> core-shell nanostructures as efficient hydrogen evolution electrocatalyst for alkaline water electrolysis. *Int J Hydrogen Energy* 2019;44:25310–8.
- [3] Song YJ, Ji KY, Duan HH, Shao MF. Hydrogen production coupled with water and organic oxidation based on layered double hydroxides. *Explorations* 2021;1:210050.
- [4] Liu SH, Xu YX, Chanda D, Tan L, Xing RM, Li X, et al. Ultrathin WS<sub>2</sub> nanosheets vertically aligned on TiO<sub>2</sub> nanobelts as efficient alkaline hydrogen evolution electrocatalyst. *Int J Hydrogen Energy* 2020;45:1697–705.
- [5] Sun YT, Xu SS, Ortíz-Ledón CA, Zhu JW, Chen S, Duan JJ. Biomimetic assembly to superplastic metal–organic framework aerogels for hydrogen evolution from seawater electrolysis. *Explorations* 2021;1:20210021.
- [6] Grigoriev SA, Fateev VN, Bessarabov DG, Millet P. Current status, research trends, and challenges in water electrolysis science and technology. *Int J Hydrogen Energy* 2020;45:26036–58.
- [7] Ji X, Liu B, Ren X, Shi X, Asiri AM, Sun X. P-doped Ag nanoparticles embedded in N-doped carbon nanoflake: an efficient electrocatalyst for the hydrogen evolution reaction. *ACS Sustainable Chem Eng* 2018;6:4499–503.
- [8] Zhang J, Wang T, Pohl D, Rellinghaus B, Dong RH, Liu SH, et al. Interface engineering of MoS<sub>2</sub>/Ni<sub>3</sub>S<sub>2</sub> heterostructures for highly enhanced electrochemical overall-water-splitting activity. *Angew Chem Int Ed* 2016;55:6702–7.
- [9] Liu SH, Li BY, Mohite SV, Devaraji P, Mao LQ, Xing RM. Ultrathin MoS<sub>2</sub> nanosheets in situ grown on rich defective Ni<sub>0.96</sub>S as heterojunction bifunctional electrocatalysts for alkaline water electrolysis. *Int J Hydrogen Energy* 2020;45:29929–37.
- [10] Zhou GY, Chen Y, Dong H, Xu L, Liu X, Ge CW, et al. Ultrafine monodisperse NiS/Ni<sub>3</sub>S<sub>2</sub> heteronanoparticles in situ grown on N-doped graphene nanosheets with enhanced electrocatalytic activity for hydrogen evolution reaction. *Int J Hydrogen Energy* 2019;44:26338–46.
- [11] Kong WS, Luan XQ, Du HT, Xia L, Qu FL. Enhanced electrocatalytic activity of water oxidation in an alkaline medium via Fe doping in CoS<sub>2</sub> nanosheets. *Chem Commun* 2019;55:2469–72.
- [12] Du HT, Kong RM, Qu FL, Lu LM. Enhanced electrocatalysis for alkaline hydrogen evolution by Mn doping in a Ni<sub>3</sub>S<sub>2</sub> nanosheet array. *Chem Commun* 2018;54:10100–3.
- [13] Guo K, Wang Y, Huang J, Lu M, Li H, Peng Y, et al. In situ activated Co<sub>3</sub>-xNi<sub>x</sub>O<sub>4</sub> as a highly active and ultrastable electrocatalyst for hydrogen generation. *ACS Catal* 2021;8:174–82.
- [14] Cui W, Cheng N, Liu Q, Ge C, Asiri AM, Sun X. Mo<sub>2</sub>C nanoparticles decorated graphitic carbon sheets: biopolymer-derived solid-state synthesis and application as an efficient electrocatalyst for hydrogen generation. *ACS Catal* 2014;4:2658–61.
- [15] Jin H, Wang X, Tang C, Vasileff A, Li L, Slattery A, et al. Stable and highly efficient hydrogen evolution from seawater enabled by an unsaturated nickel surface nitride. *Adv Mater* 2021;33:2007508.
- [16] Yu X, Xu S, Wang Z, Cheng X, Du Y, Chen G, et al. An Mn-doped NiCoP flower-like structure as a highly efficient electrocatalyst for hydrogen evolution reaction in acidic and alkaline solutions with long duration. *Nanoscale* 2021;13:11069–76.
- [17] Mohite SV, Xing RM, Li BY, Latthe SS, Zhao Y, Li XY, et al. Spatial compartmentalization of cobalt phosphide in P-doped dual carbon shells for efficient alkaline overall water splitting. *Inorg Chem* 2020;59:1996–2004.
- [18] Du HT, Kong RM, Guo XX, Qu FL, Ji JH. Recent progress in transition metal phosphides with enhanced electrocatalysis for hydrogen evolution. *Nanoscale* 2018;10:21617–24.
- [19] Guo Z, Liu L, Wang J, Cao Y, Tu J, Zhang X, et al. Recent progress in CoP-based materials for electrochemical water splitting. *Int J Hydrogen Energy* 2021;46:34194–215.
- [20] Wang H, Xiao X, Liu S, Chiang C-L, Kuai X, Peng C-K, et al. Structural and electronic optimization of MoS<sub>2</sub> edges for hydrogen evolution. *J Am Chem Soc* 2019;141:18578–84.
- [21] Yi XR, He XB, Yin FX, Chen BH, Li GR, Yin HQ. One-step synthesis of oxygen incorporated V–MoS<sub>2</sub> supported on partially sulfurized nickel foam as a highly active catalyst for hydrogen evolution. *Int J Hydrogen Energy* 2020;45:2774–84.
- [22] Zhang DW, Jiang LJ, Liu YY, Qiu LJ, Zhang JM, Yuan DS. Ni<sub>3</sub>S<sub>2</sub>-MoS<sub>x</sub> nanorods grown on Ni foam as high-efficient electrocatalysts for overall water splitting. *Int J Hydrogen Energy* 2019;44:17900–8.

- [23] Lin JH, Wang PC, Wang HH, Li C, Si XQ, Qi JL, et al. Defect-rich heterogeneous MoS<sub>2</sub>/NiS<sub>2</sub> nanosheets electrocatalysts for efficient overall water splitting. *Adv Sci* 2019;6:1900246.
- [24] An T, Wang Y, Tang J, Wei W, Cui XQ, Alenizi AM, et al. Interlaced NiS<sub>2</sub>–MoS<sub>2</sub> nanoflake-nanowires as efficient hydrogen evolution electrocatalysts in basic solutions. *J Mater Chem* 2016;4:13439–43.
- [25] Zou YJ, Xiao B, Shi J-W, Hao H, Ma DD, Lv YX, et al. 3D hierarchical heterostructure assembled by NiFe LDH/(NiFe) Sx on biomass-derived hollow carbon microtubes as bifunctional electrocatalysts for overall water splitting. *Electrochim Acta* 2020;348:136339.
- [26] Singh B, Indra A. Prussian blue- and Prussian blue analogue-derived materials: progress and prospects for electrochemical energy conversion. *Mater Today Energy* 2020;16:100404.
- [27] Guo YN, Tang J, Wang ZL, Kang Y-M, Bando Y, Yamauchi Y. Elaborately assembled core-shell structured metal sulfides as a bifunctional catalyst for highly efficient electrochemical overall water splitting. *Nano Energy* 2018;47:494–502.
- [28] Liang J, Wang YY, Liu Q, Luo YL, Li TS, Zhao HT, et al. Electrocatalytic hydrogen peroxide production in acidic media enabled by NiS<sub>2</sub> nanosheets. *J Mater Chem* 2021;9:6117–22.
- [29] Liu YK, Jiang S, Li SJ, Zhou L, Li ZH, Li JM, et al. Interface engineering of (Ni, Fe)S<sub>2</sub>@MoS<sub>2</sub> heterostructures for synergetic electrochemical water splitting. *Appl Catal, B* 2019;247:107–14.
- [30] Li Y, Yin K, Wang LL, Lu XL, Zhang Y, Liu YT, et al. Engineering MoS<sub>2</sub> nanomesh with holes and lattice defects for highly active hydrogen evolution reaction. *Appl Catal, B* 2018;239:537–44.
- [31] Shi WH, Mao J, Xu XL, Liu WX, Zhang L, Cao XH, et al. An ultra-dense NiS<sub>2</sub>/reduced graphene oxide composite cathode for high-volumetric/gravimetric energy density nickel–zinc batteries. *J Mater Chem* 2019;7:15654–61.
- [32] Long X, Li GX, Wang ZL, Zhu HY, Zhang T, Xiao S, et al. Metallic iron–nickel sulfide ultrathin nanosheets as a highly active electrocatalyst for hydrogen evolution reaction in acidic media. *J Am Chem Soc* 2015;137:11900–3.
- [33] Liu N, Guo YL, Yang XY, Lin HL, Yang LH, Shi ZP, et al. Microwave-assisted reactant-protecting strategy toward efficient MoS<sub>2</sub> electrocatalysts in hydrogen evolution reaction. *ACS Appl Mater Interfaces* 2015;7:23741–9.
- [34] Guan SD, Fu XL, Lao ZZ, Jin CH, Peng ZJ. NiS–MoS<sub>2</sub> hetero-nanosheet array electrocatalysts for efficient overall water splitting. *Sustain Energy Fuels* 2019;3:2056–66.
- [35] Yang YQ, Zhang K, Lin HL, Li X, Chan HC, Yang L, et al. MoS<sub>2</sub>–Ni<sub>3</sub>S<sub>2</sub> heteronanorods as efficient and stable bifunctional electrocatalysts for overall water splitting. *ACS Catal* 2017;7:2357–66.